

CEBAF Program Advisory Committee Nine Proposal Cover Sheet

This proposal must be received by close of business on Thursday, December 1, 1994 at:

CEBAF

User Liaison Office, Mail Stop 12 B

12000 Jefferson Avenue

Newport News, VA 23606

Proposal Title

Polarization Transfer in the ${}^3\text{He}(\bar{e}, e'\bar{p})d$
and ${}^3\text{He}(\bar{e}, e'\bar{p})pn$ Reactions

Contact Person

Name: Dr. R. D. Ransome

Institution: Rutgers University

Address: P.O. Box 844, Physics Department,

Address: Piscataway, NJ, 08855-0844

City, State ZIP/Country:

Phone: (908) 445-3873

FAX: (908) 445-4343

E-Mail → Internet: ransome@ruthep.rutgers.edu

Experimental Hall: A Days Requested for Approval: 26

Hall B proposals only, list any experiments and days for concurrent running:

CEBAF Use Only

Receipt Date: 12/15/94

PR 94-112

By: 90

Proposal for the PAC 9 of CEBAF (Jan./Feb. 1995)

Polarization Transfer in the ${}^3\text{He}(\vec{e}, e'\vec{p})d$ and ${}^3\text{He}(\vec{e}, e'\vec{p})pn$ Reactions

E.J. Brash^a (spokesperson), R.D. Ransome^a (contact person),
and P.M. Rutt^b (co-spokesperson)

^a *Rutgers University, Box 849, Piscataway, NJ, 08855.*

^b *University of Georgia, Athens, GA, 30602.*

A Hall A Collaboration Proposal

California State University Los Angeles, CEA-Saclay (France), CEBAF, Chungnam National University (Korea), College of William & Mary, Duke University, IPN Orsay (France), Kharkov Institute of Physics and Technology (Ukraine), M.I.T., Norfolk State University, Old Dominion University, Rutgers University, University of Georgia, University of Kentucky, University of Maryland, University of New Hampshire, University of Regina, University of Virginia, Yerevan Physics Institute (Armenia).

Abstract

We propose to measure the polarization transfer coefficients, D_{ll} and D_{ll} , as well as the induced normal polarization, P_n , in the ${}^3\text{He}(\vec{e}, e'\vec{p})d$ and ${}^3\text{He}(\vec{e}, e'\vec{p})pn$ reactions simultaneously. Recent calculations of the polarization transfer coefficients in the ${}^3\text{He}(\vec{e}, e'\vec{p})d$ reaction at low missing momentum have shown that the ratio of these observables is insensitive to the details of the ${}^3\text{He}$ wavefunction and hence provides a measure of the bound proton form factor ratio, G_M^p/G_E^p . In contrast, calculations indicate that the polarization transfer coefficients in the ${}^3\text{He}(\vec{e}, e'\vec{p})pn$ reaction are very sensitive to the S' -state contributions to the ${}^3\text{He}$ ground state wavefunction at low recoil momentum. The measurement of the induced normal polarization will provide an indication of the size of final state interaction effects.

We will measure these observables as a function of the missing momentum, p_m , over the range $0 < p_m < 250$ MeV/c, for values of Q^2 of 0.8, 1.5, 3.0, and 4.0 (GeV/c)². Since a single kinematical configuration will be used at each value of Q^2 and because the ratio of polarization transfer coefficients is independent of the incident electron polarization and of the carbon analyzing power in the focal plane polarimeter, it is anticipated that the systematic uncertainties will be minimized.

December 14, 1994

1 Physics Motivation.

In this experiment we propose to use the ${}^3\text{He}(\vec{e},e'\vec{p})d$ and ${}^3\text{He}(\vec{e},e'\vec{p})pn$ reactions to measure the spin transfer coefficients, D_{ll} and D_{lt} , as well as the induced normal polarization, P_n . Our study of the ${}^3\text{He}$ nucleus using polarization transfer is motivated by several factors. In the ${}^3\text{He}(\vec{e},e'\vec{p})d$ reaction, the ratio of spin transfer coefficients is directly related to the ratio of the Sachs electromagnetic form factors for the proton, G_M^p/G_E^p , and therefore we will investigate possible medium modification of this ratio in a way which eliminates many of the systematic uncertainties which are typical of cross-section measurements. The physics program in Hall A currently includes approved experiments which will be sensitive to the ratio of proton electromagnetic form factors in ${}^1\text{H}$, ${}^2\text{H}$, and ${}^4\text{He}$. This experiment would complete the systematic study of possible medium modification effects for light nuclei. Due to the rapid change in binding energy per nucleon, it is expected that medium effects will vary strongly with A over this range of nuclei. In addition, exact microscopic calculations are available for all of these nuclei. In the ${}^3\text{He}(\vec{e},e'\vec{p})pn$ reaction, the polarization transfer coefficients are very sensitive to the S' -state contributions to the ${}^3\text{He}$ ground state wavefunction at low recoil momentum. Because we can now solve the corresponding Faddeev equations for the three-body system exactly, the ${}^3\text{He}$ nucleus provides an excellent testing ground for our understanding of the physics of the NN and NNN forces. As will be described in more detail in Section 1.2, the S' component in ${}^3\text{He}$ is directly related to the binding energy of the three-body systems, which has been a long standing problem in models of three-body systems which do not include relativistic effects, three-body forces, NN- $N\Delta$ couplings, or non-nucleonic degrees of freedom.

1.1 Medium Modification of Ratio of Proton Electromagnetic Form Factors in Nuclei

During the past twenty years, inclusive and exclusive electron scattering experiments have been used to gain much information on the structure of nuclei as well as on the electron-nucleus reaction mechanism. Within the nucleon-meson picture of nuclei, the usual assumption made in most calculations is that the incident electron interacts with a single nucleon

- the Impulse Approximation (IA). However, recent experiments have indicated that the IA may be inadequate in certain kinematic regimes. Inclusive electron scattering experiments for a range of nuclei at MIT [1], Saclay [2, 3, 4], and SLAC [5, 6] have shown that, except in ${}^3\text{He}$ and ${}^4\text{He}$, a considerable amount of longitudinal strength is missing. In exclusive $(e, e'p)$ experiments [7, 8, 9, 10] on ${}^6\text{Li}$, ${}^{12}\text{C}$, and ${}^{40}\text{Ca}$, the ratio of electromagnetic form factors of the bound proton, G_M^p/G_E^p , differs significantly from the free proton value, as shown in Figure 1.

The deviations from the free proton value for this ratio may be due to medium modification of the spinors, current operators, or nucleon form factors. Celenza *et al.* have considered a non-topological soliton model of the nucleon [11]. Within this model, the quarks within the nucleon couple to the meson fields as well as an additional scalar field introduced to provide quark confinement. The result is a reduction of the constituent quark masses, and hence an increased charge radius of the proton. Along the same lines, Mulders [12] has used a Fermi Gas model of the nucleon to show that the nucleon size (and hence the proton charge radius) is significantly enhanced in the nuclear medium. Carlson and Haven [13] suggest that the deviation is due to formation of six-quark clusters at large nuclear densities.

Others [14, 15, 16] have indicated that the enhancement may be associated with final state interaction or meson exchange current effects. To support this, a recent calculation by Krewald [17] which takes into account quark degrees of freedom indicates that at nuclear matter densities Pauli blocking effects which had not been taken into account previously result in a significant *reduction* of the nucleon size and hence would tend to cancel the predicted increase in size of the nucleon in the soliton model. In a microscopic calculation by Carlson and Schiavilla [18] which includes pion degrees of freedom, both the longitudinal and transverse responses agree well with the experimental data for inclusive (e, e') scattering from ${}^4\text{He}$ at low Q^2 . Interestingly, the agreement for ${}^3\text{He}$ calculated in the same framework is not as good.

In the cross-section measurements to date, it has been difficult to separate such reaction mechanism effects from medium modification effects. Therefore, as an important step in the systematic investigation of the possible modification of the proton electromagnetic form factors in nuclei, we propose to measure the polarization transfer coefficients, $D_{||}$ and D_{\perp} ,

as well as the induced normal polarization, P_n , in the ${}^3\text{He}(\vec{e}, e'\vec{p})d$ reaction. There are a number of factors which make ${}^3\text{He}$ an interesting nucleus for this study. An important point is that all of the explanations which predict a modification of the electromagnetic form factors of the bound proton in the nuclear medium suggest a strong density dependence. Thus a direct comparison between a relatively low density nucleus such as ${}^3\text{He}$, where exact wavefunction calculations are available, and a high density nucleus such as ${}^4\text{He}$ would be desirable. Since we have chosen identical kinematics for this experiment as for the approved CEBAF Experiment 93-049, which will measure the form factor ratio in the ${}^4\text{He}(\vec{e}, e'\vec{p}){}^3\text{H}$ reaction [19], such a comparison would be possible.

Thus, if the proton electromagnetic form factors are indeed modified in the nuclear medium, the effect should be much more pronounced in ${}^4\text{He}$ than in ${}^3\text{He}$. Indeed, from $A=1$ to $A=4$ the binding energy per nucleon increases rapidly, and hence we would expect medium modification effects to begin to manifest themselves over this range of nuclei. In this scenario, ${}^3\text{He}$ would serve as an important benchmark in the study of form factors in nuclei. In contrast, reaction mechanism effects could lead to a significant enhancement of this ratio in *both* ${}^3\text{He}$ and ${}^4\text{He}$. As well, deviations of the ratio from the free value could be indicative that relativistic effects are becoming important at these momentum transfers, especially since the only calculations that presently exist for ${}^3\text{He}$ indicate that meson exchange current and final state interaction effects are small in this kinematic regime.

A detailed analysis of the polarization response functions in $(\vec{e}, e'\vec{p})$ scattering has been developed by Picklesheimer and Van Orden [20]. Their analysis shows that there are 18 independent response functions. The polarization of the outgoing proton, \mathbf{S} , in the process $e^- + {}^3\text{He} \rightarrow e^- + p + d$ is defined by:

$$\begin{aligned} \frac{d^3\sigma}{d\omega d\Omega_e d\Omega_p} &= \frac{m_p |\mathbf{p}|}{2(2\pi)^3} \left[\frac{d\sigma}{d\Omega_e} \right]_{Mott} \times (v_L(R_L + R_L^n S_n) + v_T(R_T + R_T^n S_n) \\ &+ v_{TT} \left[(R_{TT} + R_{TT}^n S_n) \cos(2\phi) + (R_{TT}^l S_l + R_{TT}^t S_l) \sin(2\phi) \right] \\ &+ v_{LT} \left[(R_{LT} + R_{LT}^n S_n) \cos(\phi) + (R_{LT}^l S_l + R_{LT}^t S_l) \sin(\phi) \right] \\ &+ h v_{LT'} \left[(R_{LT'} + R_{LT'}^n S_n) \sin(\phi) + (R_{LT'}^l S_l + R_{LT'}^t S_l) \cos(\phi) \right] \\ &+ h v_{TT'} (R_{TT'}^l S_l + R_{TT'}^t S_l) \end{aligned} \quad (1)$$

Here $\omega = E - E'$ is the energy loss of the incident electron, \mathbf{p} is the 3-momentum of

the proton in the centre-of-mass system (CMS) of $\gamma^* + {}^3\text{He} \rightarrow p + d$, $d\Omega_e$ ($d\Omega_p$) is the element of solid angle in the lab system (CMS), h is the helicity of the initial electron, and ϕ is the azimuthal angle between the electron scattering plane and the plane formed by the virtual photon momentum, \mathbf{q} , and \mathbf{p} . The v 's are kinematic factors weighting the various virtual photon polarization states and $[d\sigma/d\Omega_e]_{Mott}$ is the cross-section for scattering from a structureless Dirac particle. The direction l is along the momentum of the scattered proton, n is normal to the reaction plane, and t is perpendicular to both l and n .

This expression assumes the conservation of electromagnetic current for $\gamma^* + {}^3\text{He} \rightarrow p + d$, the validity of the one-photon mechanism for $e^3\text{He} \rightarrow epd$, and parity conservation in the strong and electromagnetic interactions. Moreover, the formula should hold for any process $A(e, e'p)X$, the specifics of each process being contained in the helicity amplitudes of $\gamma^* + A \rightarrow p + X$. The response functions, R , can in turn be expressed in terms of the 18 helicity amplitudes of the reaction $\gamma^* + {}^3\text{He} \rightarrow p + d$ or the 24 helicity amplitudes of the reaction $\gamma^* + {}^3\text{He} \rightarrow p + p + n$.

For coplanar kinematics, where the outgoing proton is emitted in the scattering plane, only twelve of the response functions of Equation 1 survive. In terms of the *polarization dependent* part of cross-section, σ_{pd} , the components of the proton polarization are given by

$$\begin{aligned}
\sigma_{pd}S_l &= h \frac{m_p |\mathbf{p}|}{2(2\pi)^3} \left[\frac{d\sigma}{d\Omega_e} \right]_{Mott} (v_{TT} R_{TT}^l + v_{LT} R_{LT}^l \cos(\phi)) \\
\sigma_{pd}S_n &= \frac{m_p |\mathbf{p}|}{2(2\pi)^3} \left[\frac{d\sigma}{d\Omega_e} \right]_{Mott} (v_L R_L^n + v_T R_T^n + v_{TT} R_{TT}^n \cos(2\phi) + v_{LT} R_{LT}^n \cos(\phi)) \quad (2) \\
\sigma_{pd}S_t &= h \frac{m_p |\mathbf{p}|}{2(2\pi)^3} \left[\frac{d\sigma}{d\Omega_e} \right]_{Mott} (v_{TT} R_{TT}^t + v_{LT} R_{LT}^t \cos(\phi))
\end{aligned}$$

It is interesting to note that the response functions R_L^n , R_T^n , R_{TT}^n , and R_{LT}^n are given by imaginary parts of bilinear combinations of helicity amplitudes. In the PWIA, the helicity amplitudes are real and therefore these structure functions, and hence the normal component of the polarization, is zero.

The components of the outgoing proton polarization with respect to the momentum

transfer, \mathbf{q} , are given by

$$\begin{bmatrix} P_x \\ P_y \\ P_z \end{bmatrix} = \begin{pmatrix} \sin(\theta_{pq}) & 0 & \cos(\theta_{pq}) \\ 0 & 1 & 0 \\ \cos(\theta_{pq}) & 0 & -\sin(\theta_{pq}) \end{pmatrix} \begin{bmatrix} S_t \\ S_n \\ S_l \end{bmatrix} \quad (3)$$

where z is along the momentum transfer, y is perpendicular to the electron scattering plane, and x is perpendicular to both z and y . θ_{pq} is the angle between the outgoing proton and the momentum transfer.

According to Equation 2, the longitudinal and transverse components of the outgoing proton polarization in the ${}^3\text{He}(\vec{e},e'\vec{p})d$ reaction are non-zero in the PWIA and are proportional to the electron beam helicity. Therefore, one may write

$$S_t = hD_{tt} \quad (4)$$

$$S_l = hD_{ll}$$

where D_{tt} and D_{ll} are the so-called spin transfer coefficients.

In the PWIA and collinear kinematics, D_{tt} and D_{ll} may be expressed in terms of the bound proton electromagnetic form factors, G_{Ep} and G_{Mp} , as [21, 22]

$$I_0 D_{tt} = -2(\tau(1+\tau))^{\frac{1}{2}} G_{Mp} G_{Ep} \tan\left(\frac{\theta_e}{2}\right) \quad (5)$$

$$I_0 D_{ll} = \frac{E+E'}{m_p} (\tau(1+\tau))^{\frac{1}{2}} G_{Mp}^2 \tan^2\left(\frac{\theta_e}{2}\right) \quad (6)$$

$$I_0 = G_{Ep}^2 + \tau G_{Mp}^2 \left[1 + 2(1+\tau) \tan^2\left(\frac{\theta_e}{2}\right) \right]$$

where $\tau = \frac{Q^2}{4m_p^2}$. Using this description, one sees that the ratio of the longitudinal and transverse components of the recoil proton polarization is proportional to the ratio of the magnetic and electric proton form factors, as

$$\frac{S_l}{S_t} = -\frac{E+E'}{2m_p} \tan\left(\frac{\theta_e}{2}\right) \frac{G_{Mp}}{G_{Ep}} \quad (7)$$

As noted above, this expression is valid only in the PWIA with single nucleon knockout. Thus we expect that the equality should hold in the low missing momentum region ($p_m < 200$ MeV/c) where the polarization observables in the ${}^3\text{He}(\vec{e},e'\vec{p})d$ reaction are insensitive to

S' - and D-state components in the ${}^3\text{He}$ ground state wavefunction as well as final state interaction and meson exchange effects. This is shown in Figures 2a and 2b, where we also show the predicted uncertainties of our planned data points. The incident electron energy is 4 GeV and the curves are for the lowest value of Q^2 of $0.8 (\text{GeV}/c)^2$. The solid curves, which include final state interaction and meson exchange current effects, are calculations by Laget [27] and use the full ${}^3\text{He}$ wavefunction of Reference [28]. The dashed curves have FSI/MEC effects removed. The effect of removing S' - and D-states from the full ${}^3\text{He}$ wavefunction is negligible. The calculations indicate that the polarization transfer coefficients are not strongly varying functions of the recoil momentum.

The above equation indicates that the measurement of this ratio only requires an accurate knowledge of the incident and scattered electron energies, the electron scattering angle, and the spin precession angle, χ , of the recoil proton polarization in the spectrometer. Because these quantities will be measurable to high precision, the experimental uncertainty in the ratio of the form factors is dominated by the uncertainty in the ratio of the polarization observables. This ratio is independent of the electron polarization and of the analyzing power in the focal plane polarimeter.

1.2 Small Components of the ${}^3\text{He}$ Ground State Wavefunction

Few body systems have always played a special role in nuclear physics. The goal has been to solve numerically the Schrödinger equation for nuclear Hamiltonians based on realistic nuclear potentials. This has been accomplished for the deuteron and for the $A=3$ systems, for the latter by solving the corresponding Faddeev equations.

The physical problem is enormously simplified by suppressing non-nucleonic degrees of freedom, considering only non-relativistic dynamics, and assuming that nucleons interact primarily via two-body forces. Despite these simplifications, such a model describes much experimental data amazingly well. Due to the success of the model, most efforts have focussed on extensions of it, by including meson exchange currents, three-body forces, NN- $N\Delta$ couplings, relativistic dynamics, and non-nucleonic degrees of freedom such as the quark-gluon substructure of hadrons [23, 24, 25].

Within this non-relativistic model containing only two-body forces, no approximations

are made, and therefore, disagreement between theory and experiment is indicative of missing physics. Also, once accurate models of few-nucleon systems are created one can test our understanding of benchmark calculational methods which may prove effective in many-nucleon systems.

One of the long standing benchmarks used in evaluating calculations using realistic NN potentials in the $A=3$ systems is the triton binding energy. In models where only two-body forces are included the triton is underbound, even when up to 34 NN potential waves are retained [26, 28, 29, 30]. There have been many suggestions as to the origin of this discrepancy, the most common being the lack of multi-nucleon or specifically three-body forces. Indeed, experimentally there have been a number of cases reporting large discrepancies between three-nucleon data and calculations which include only two-body forces. Ruth *et al.* [31] have measured cross-sections in the ${}^3\text{He}(\gamma,p)$ reaction. Calculations by Laget [32] which include some three-body force terms are in much better agreement with the data than two-body calculations in the 'dip' region between the quasielastic and delta regions.

A similar situation is seen in the exclusive ${}^3\text{He}(\gamma,pp)$ reaction, where the cross-section is predicted, in two-body force models, to be extremely small above 300 MeV/c recoil momentum. Sarty [33] and Audit *et al.* [34] have measured this cross-section for $W_{pp}=2010$, 2040, and 2160 MeV, where W_{pp} is the total energy of the two protons in the centre-of-mass system. The data, which are shown in Figure 3, fall well above the two-body force calculations, but are in qualitative agreement with three-body calculations of Laget [35].

Unfortunately, in the case of the triton binding energy, the agreement is not as good. Adding a static three-body force enhances the ${}^3\text{H}$ binding; however, the results are extremely sensitive to the cutoff in the πN form factor used. In general, three-body force models which use a consistent πN form factor cutoff for all Feynman diagrams considered overbind the $A=3$ systems [36, 37, 38, 39].

The wavefunction probabilities, P_S , $P_{S'}$, P_P , and P_D , are not physical observables. However, they provide a useful characterization of the wavefunction generated by a particular force model. In a central force approximation, $P_{S'}=0$ implies that $V({}^1S_0)=V({}^3S_1)$. The mixed symmetry S' -state provides a measure of the difference that exists between the ${}^3\text{H}$

and ${}^3\text{He}$ wavefunctions due to the fact that the NN force is charge dependent. The S' -state corresponds to an excitation in oscillator language from the $(1s)^3$ configuration to the $(1s)^2(2s)$ or $(1s)(1p)^2$. This implies that $P_{S'}$ should vary as the inverse square of the binding energy. Thus, there is a direct connection between $P_{S'}$ and the binding energy in the $A=3$ systems.

Models which include new physics such as three-body forces or NN- $N\Delta$ couplings that enhance the triton binding energy necessarily decrease $P_{S'}$. This is shown [23] in Figure 4. In the plot of the S' -state probability versus the binding energy of the triton in that particular force model, it is seen that the relationship $P_{S'} \sim (E_B)^{-2.1}$ is followed. The two-body force models which underbind the triton give a larger S' -state probability than the three-body force models which overbind it.

Calculations of the spin transfer coefficients, D_{it} and D_{ti} , in the ${}^3\text{He}(\vec{e}, e'\vec{p})pn$ three-body breakup reaction do not exist at this time. However, we may gain some insight into the sensitivity of this reaction to the S' -state contribution in the ${}^3\text{He}$ wavefunction by looking at calculations of the target related asymmetries, A'_x and A'_z in the ${}^3\vec{\text{He}}(\vec{e}, p)pn$ reaction (See Figure 5). From time reversal symmetry we have that, at zero recoil momentum, $A'_x = P_x$ and $A'_z = -P_z$ [22]. Therefore, if we are sensitive to the S' -state component in the target related asymmetries at low missing momenta, we expect the same sensitivity in the spin transfer coefficients.

In Figure 5, the calculations of Laget [40] are shown. While the solid, long-dashed, and dash-dot curves include the S' -state contribution to the ${}^3\text{He}$ wavefunction, the dotted curves are for $P_{S'}=0$. The observable A'_x in the ${}^3\vec{\text{He}}(\vec{e}, p)pn$ reaction (and hence P_x in the ${}^3\text{He}(\vec{e}, e'\vec{p})pn$ reaction) at low missing momenta is most sensitive to the S' -state contribution to the ${}^3\text{He}$ wavefunction. As mentioned previously, one is insensitive to this component in the ${}^3\text{He}(\vec{e}, e'\vec{p})d$ reaction, indicating that the contributions from the various helicity amplitudes for the two-body- and three-body-breakup reactions differ significantly.

The total S' -state probability in the ${}^3\text{He}$ ground state wavefunction is given by the integral over all possible recoil momenta of $|\psi_{S'}(p_R)|^2$, where $\psi_{S'}$ is the S' -state admixture to the ${}^3\text{He}$ wavefunction. Even without calculations of the recoil momentum dependence of the polarization observables at this time, we may make some estimates of our sensitivity

in this experiment to this component of the wavefunction. At zero recoil momentum, we see that the polarized target asymmetry, A'_x varies by a factor of two depending on the S' contribution. The expected error bars on our data points for the corresponding polarization observable, P_x , are comparable in this region of recoil momentum to those shown in Figure 2. Thus we expect that we would be able to determine the S' -state admixture to the ^3He wavefunction to within $\sim 10\%$ at zero recoil momentum.

2 The Experiment

2.1 Introduction

The experiment is proposed for the CEBAF electron-scattering facility using the Hall A high resolution spectrometers. An incident electron beam with an energy of 4 GeV and 100% duty factor will be used. We will measure simultaneously the polarization transfer coefficients, D_{ll} and D_{lt} , in the reactions $^3\text{He}(\vec{e},e'\vec{p})d$ and $^3\text{He}(\vec{e},e'\vec{p})pn$. In addition, we will measure the induced normal polarization, P_n . These coefficients will be measured over a large range of missing momentum ($0 < p_m < 250$ MeV/c) at values of Q^2 of 0.8, 1.5, 3.0, and 4.0 (GeV/c)². The expected combined missing energy resolution of ~ 1 MeV of the Hall A spectrometers will allow a clean separation of the two-body and three-body breakup channels.

2.2 The High-Pressure ^3He Gas Target Cell

A high-pressure gas target cell is being developed by Rutgers University. The target, which will be operated at a pressure of 150 atmospheres and a temperature of 280 K, is depicted in Figure 6. The target density corresponding to this temperature and pressure is 19.6 mg/cm³. Assuming that there will be available 67 μA of 45% longitudinally polarized electrons to the Hall, the resulting luminosity is 8.2×10^{37} cm⁻²s⁻¹.

The side windows of the target are formed by seamless Al tube, approximately 50 cm long, with an outer diameter of 0.500" and a wall thickness of 0.028". This tubing will be inserted into a piece of 3.5" dia. cylindrical Al stock which has been drilled along its length

to accommodate the tube. Material on the sides of this piece will be removed (except at the ends) to expose the surface of seamless Al tubing. This cylindrical Al stock will have cooling manifolds mounted on it and a chilled water supply will maintain the target cell at room temperature. A $67 \mu\text{A}$ electron beam will deposit about 200 W of heat when the target is operated at 150 atm. The target cell will be closed at each end by a piece of Al stock which will form the end window and provide a gas fill port. These two Al endpieces will each have a 0.500" diameter region machined to provide 0.030" thick end windows for the target cell.

The connections between the seamless tube, the cylindrical stock to which the cooling manifolds are mounted, and the endpieces will be formed by electron beam welds at each interface. These welds will be hydrostatically tested to determine a safe operating pressure and tested at high pressure with helium gas to check the porosity of the weld. The seamless Al tubing has been certified by the vendor to have a burst strength of ~ 400 atm. Test stands for the hydrostatic and helium leak measurements have been assembled at Rutgers and evaluation of target cell components is underway.

Preliminary calculations of equilibrium gas cell temperatures and endwindow heating indicate that effects due to beam heating will fall within the projected operating range for this target cell. More detailed calculations are underway. Since the gas in the target cell is not being flowed, local density fluctuations will occur at some level. Again, because in this experiment we will measure polarization observables and not absolute cross-sections, such fluctuations will not affect our results. It is also anticipated that density fluctuations will not strongly affect the average data acquisition rate.

For the experiment, three such cells will be mounted on top of the solid target ladder along with a support/alignment structure mounted on the platform of the scattering chamber. The targets will be positioned by the actuator of the existing solid target ladder. One cell will be filled with ^3He for the experiment and another will be filled to a pressure of 10 atm with hydrogen. This cell will be used to calibrate the coincidence detection efficiency using the $^1\text{H}(e,e'p)$ reaction. A third cell will be empty and will be used for background studies.

Due to the 50 cm active length of the target cell, neither the entrance or exit windows are

within the acceptance of either spectrometer for the kinematics chosen. Backgrounds from photoproduction in the entrance window will be eliminated by requiring the electron-proton coincidence.

2.3 The Focal Plane Polarimeter

The focal plane polarimeter intended for the Hall A hadron spectrometer is under construction at Rutgers University and the College of William & Mary. The polarimeter will determine the proton polarization through the azimuthal asymmetry induced in scattering the proton from a carbon analyzer, as in previous polarimeters at hadron facilities. Four straw-tube chambers are used to track the proton trajectory into and out of a graphite block. False asymmetries will be minimized due to the chamber resolution ($\sigma < 250\mu\text{m}$), small multiple scattering at higher energies, and the continuous alignment information provided by the spectrometer high resolution front chambers. Tracking efficiency is estimated to be about 99% for single-track events.

After the proton travels through the spectrometer, the components of its polarization normal to the bend plane (Y) and along the momentum dispersion direction (X) are measured in the polarimeter. Unlike the normal and longitudinal components, the sideways component of the proton polarization immediately after scattering does not precess (to first order) in the magnetic field of the spectrometer. If the precession angle in the spectrometer is given by χ , then the polarization components measured at the polarimeter are given in terms of the polarization components immediately after scattering (as in Equation 2 above) by

$$\begin{aligned} P_X &= S_n \cos(\chi) + S_l \sin(\chi) \\ P_Y &= S_l. \end{aligned} \tag{8}$$

The precession angle is given by

$$\chi = \frac{g-2}{2} \gamma \Omega_B, \tag{9}$$

where g is the proton gyromagnetic ratio (5.586), γ is the Lorentz factor and Ω_B is the bend angle of the proton in the spectrometer. The three components of the proton polarization

Table 1: Kinematics for the Proposed Experiment

Q^2 (GeV/c) ²	E (GeV)	E' (GeV)	θ_e (deg)	T_p (GeV)	θ_p (deg)
0.8	4.0	3.57	13.59	0.424	58.14
1.5	4.0	3.20	19.70	0.795	47.76
3.0	4.0	2.40	32.46	1.594	33.21
4.0	4.0	1.87	42.91	2.130	25.80

at the target are determined uniquely using the fact the P_y is independent of the electron helicity.

3 Count Rate and Beam Time Estimates

3.1 Kinematics

We have chosen to measure the spin transfer coefficients at four values of Q^2 , namely 0.8, 1.5, 3.0, and 4.0 (GeV/c)². As can be seen in the calculations of these observables, final state interaction and meson exchange current effects should be small at these momentum transfers. As mentioned previously, these kinematics are identical to those of CEBAF proposal 93-049, which will measure the same observables in the ${}^4\text{He}(\vec{e}, e'\vec{p}){}^3\text{H}$ reaction [19]. The kinematics are given in Table 1.

3.2 Count Rate Estimates

The count rates for the present experiment were calculated using the Monte Carlo reaction code MCEEP [41]. The acceptances of each spectrometer are $\delta\theta = \pm 27$ mr, $\delta\phi = \pm 65$ mr, and $\delta p = \pm 5\%$. The pressure of the ${}^3\text{He}$ target is 150 atm at 280 K, and the target length is 50 cm. This corresponds to a luminosity of 8.2×10^{37} cm⁻²s⁻¹ assuming 67 μA of 45% longitudinally polarized electrons. In practice, however, the acceptances of the spectrometers are ± 5 cm at 90°, and therefore the effective luminosity for coincidence measurements is reduced. The

effective luminosity in the kinematics chosen is shown in Table 2. Also shown in the table are the total counts predicted in the two-body and three-body breakup channels for each missing momentum bin. For both channels, the spectral function of Meier-Hadjuk *et al.* [42] was used.

3.3 Background Estimates

As mentioned previously, the endcaps of the target cell will be outside of the acceptances of both spectrometers in the chosen kinematics. Thus the main sources of background are random coincidences from singles scattering in the target. The singles rates for (e,e') , (e,π^-) , (e,p) , and (e,π^+) are shown in Table 3, along with the real to accidental ratio assuming a time-of-flight window of 2 ns and a duty factor of 100%. These rates were also calculated with MCEEP. The Cerenkov and shower counters will be used for particle identification, and will serve to reject a large fraction of the random coincidences for pion events. The real to accidental rate shown could also be improved using a software cut on the correlated vertex position. Such a cut could improve this ratio by at least an order of magnitude.

3.4 Statistical and Systematic Uncertainties

The statistical uncertainties for the polarization observables shown in Figures 2a, 2b, 5a, and 5b were calculated in the following manner. The percentage of protons scattering in the carbon analyzer of the FPP into an angular cone from 5° to 20° is estimated using either a parametrization of the POMME data [43] or a fit to the data of Aprile-Giboni *et al.* [44], depending on the incident proton kinetic energy. The average carbon analyzing power over this angular range is taken from either the POMME parametrization or a fit to the data of McNaughton *et al.* [45], again depending on the incident proton kinetic energy. The analyzer thickness is chosen to maximize the the figure of merit for the polarimeter, $A_y^2 f$, for each kinematic point. The values of analyzer thickness, average carbon analyzing power, and fraction of events scattering into the fiducial angular cone are given in Table 4.

The uncertainty in the polarization observables measured at the polarimeter is then

Table 2: Coincidence Totals for the Proposed Experiment

Q^2 (GeV/c) ²	Beamtime (hrs)	L_{eff} (cm ⁻² s ⁻¹)	p_m (MeV/c)	θ_{pq} (°)	N_d	N_{pn}
0.8	72	1.9×10^{37}	0-50	1.63	3.67×10^8	1.82×10^8
			50-100	3.30	9.38×10^8	5.18×10^8
			100-150	5.22	4.39×10^8	3.08×10^8
			150-200	7.75	8.11×10^7	6.62×10^7
			200-250	11.14	7.20×10^6	8.32×10^6
1.5	72	2.2×10^{37}	0-50	1.07	2.71×10^7	1.38×10^7
			50-100	2.34	6.72×10^7	4.00×10^7
			100-150	3.91	4.05×10^7	3.14×10^7
			150-200	5.43	1.44×10^7	1.35×10^7
			200-250	7.41	2.08×10^6	1.88×10^6
3.0	216	3.0×10^{37}	0-50	0.69	8.93×10^6	4.16×10^6
			50-100	1.40	2.27×10^7	1.23×10^7
			100-150	2.21	1.29×10^7	9.76×10^6
			150-200	3.12	3.63×10^6	3.06×10^6
			200-250	4.24	4.84×10^5	4.61×10^5
4.0	216	2.4×10^{37}	0-50	0.55	1.64×10^6	7.49×10^5
			50-100	1.13	4.07×10^6	2.38×10^6
			100-150	1.80	2.27×10^6	1.66×10^6
			150-200	2.45	6.39×10^5	5.77×10^5
			200-250	3.36	8.70×10^4	9.08×10^4

Table 3: Single Rates for the Proposed Experiment

Q^2 (GeV/c) ²	N(e,e') Hz	N(e, π^-) Hz	N(e,p) Hz	N(e, π^+) Hz	R/A
0.8	1.2×10^5	3.9×10^3	2.2×10^4	1.3×10^4	1209
1.5	1.2×10^4	7.5×10^3	6.9×10^4	2.7×10^4	312
3.0	784	1.8×10^4	1.1×10^5	3.2×10^4	362
4.0	141	1.7×10^4	1.3×10^5	1.8×10^4	312

Table 4: Polarimeter Parameters for the Proposed Experiment

Q^2 (GeV/c) ²	Analyzer Thickness (cm)	Average A_y	f
0.8	20	.371	.08
1.5	30	.232	.18
3.0	40	.160	.22
4.0	60	.110	.44

calculated according to

$$\begin{aligned}
\delta p &= \left[\left(\frac{\delta A_y}{A_y} \right)^2 P^2 + \frac{\pi^2 ab P^2}{(a-b)^2(a+b)} \right]^{\frac{1}{2}}, \\
a &= fN(1 - PA_y), \\
b &= fN(1 + PA_y).
\end{aligned}
\tag{10}$$

The uncertainty in the polarization observables at the target are then calculated using Equation 3, Equation 4, and Equation 8.

As mentioned previously, the measurement of the ratio of bound proton form factors, G_M^p/G_E^p , is independent of the electron beam polarization and the carbon analyzing power in the focal plane polarimeter. Hence the uncertainty in the ratio will be dominated by statistics in this experiment. In contrast, for our measurement of the polarization observables in the ${}^3\text{He}(\vec{e}, e'\vec{p})pn$ reaction, we require an accurate measurement of both of these quantities. For the electron polarization, this will be accomplished using the Moeller polarimeter in Hall A, which at this beam current is expected to determine the electron polarization to within 3% of its value. For our lowest value of $Q^2=0.8$ (GeV/c) 2 , the carbon analyzing power is well determined ($\delta A/A \sim 4\%$) from the data of McNaughton *et al.*[45]. For the higher Q^2 points, the analyzing power will be accurately determined from the calibration of the polarimeter in the approved CEBAF experiment, 93-027. The expected uncertainties following calibration are 1.3% at $Q^2=1.5$ (GeV/c) 2 , 1.8% at $Q^2=3.0$ (GeV/c) 2 , and 3.9% at $Q^2=4.0$ (GeV/c) 2 .

3.5 Beam Time Request

The total beam time required is 624 hours, which includes 48 hours for setup and testing of the experimental equipment. The time required at each value of Q^2 , along with the predicted statistical uncertainty in the ratio, D_{ll}/D_{lt} , is shown in Table 5.

Table 5: Required Beam Times for the Proposed Experiment

Q^2 (GeV/c) ²	Beam Time (hours)	Statistical Uncertainty in D_u/D_u (%)
0.8	72	2.2
1.5	72	4.4
3.0	216	6.1
4.0	216	8.3

References

- [1] K.A. Dow, Ph.D. Thesis, Massachusetts Institute of Technology, (1987).
- [2] Z.-E. Meziani *et al.*, Phys. Rev. Lett. **54** (1985) 1233.
- [3] P. Barreau *et al.*, Nuclear Physics **A402** (1983) 515.
- [4] C. Marchand *et al.*, Phys. Lett. **153B** (1985) 29.
- [5] J.P. Chen *et al.*, Phys. Rev. Lett. **66** (1991) 1283.
- [6] Z.-E. Meziani *et al.*, Phys. Rev. Lett. **69** (1992) 41.
- [7] P.E. Ulmer *et al.*, Phys. Rev. Lett. **59** (1987) 2259.
- [8] G. van der Steenhoven *et al.*, Phys. Rev. Lett. **58** (1987) 1727.
- [9] D. Reffay-Pikeroen *et al.*, Phys. Rev. Lett. **60** (1988) 776.
- [10] A. Magnon *et al.*, Phys. Lett. **222B** (1989) 352.
- [11] L.S. Celenza *et al.*, Phys. Rev. Lett. **53** (1984) 892.
- [12] P.J. Mulders, Phys. Rev. Lett. **54** (1985) 2560.
- [13] C.E. Carlson and T.J. Haven, Phys. Rev. Lett. **51** (1983) 261.
- [14] T.D. Cohen *et al.*, Phys. Rev. Lett. **59** (1987) 1267.
- [15] T. Suzuki, Phys. Rev. **C37** (1988) 549.
- [16] M. Kohno, Phys. Rev. **C38** (1988) 584.
- [17] S. Krewald, Phys. Lett. **222B** (1989) 338.
- [18] J. Carlson and R. Schiavilla, Phys. Rev. **C49** (1994) R2880 and Private Communication.
- [19] CEBAF Proposal 93-049 - J.F.J. van den Brand, R. Ent, and P.E. Ulmer, cospokespersons.

- [20] A. Picklesheimer and J.W. Van Orden, Phys. Rev. C40 (1989) 290.
- [21] N. Dombey, Rev. Mod. Phys. **41** (1969) 236.
- [22] A.I. Akheizer and M.P. Rekalov, Sov. J. Part. Nucl. **4** (1974) 277.
- [23] B.F. Gibson, Nuclear Physics **A543** (1992) 1c.
- [24] A.D. Jackson and J.A. Tjon, Phys. Rev. C37 (1988) 1729.
- [25] H. Pöpping, P.U. Sauer, and Zheng Xi-Zhen, Nuclear Physics **A474** (1987) 557.
- [26] J.L. Friar *et al.*, Phys. Rev. C37 (1988) 2869.
- [27] J.M. Laget, Private Communication.
- [28] C. Hadjuk and P.U. Sauer, Nuclear Physics **A369** (1981) 361.
- [29] A. Bömelburg, Phys. Rev. C28 (1983) 403.
- [30] R.A. Brandenburg *et al.*, Phys. Rev. C37 (1988) 1245.
- [31] C. Ruth *et al.*, Phys. Rev. Lett. **72** (1994) 617.
- [32] J.M. Laget, Nuclear Physics **A497** (1989) 391.
- [33] A. Sarty, Nuclear Physics **A543** (1992) 49.
- [34] G. Audit *et al.*, Phys. Rev. C44 (1991) R575.
- [35] J.M. Laget, Phys. Rep. 69 (1981) 1 and Private Communication.
- [36] J.L. Friar *et al.*, Phys. Rev. C36 (1987) 1138.
- [37] S.A. Coon and W. Glöckle, Phys. Rev. C23 (1981) 1790.
- [38] H.T. Coelho *et al.*, Phys. Rev. C31 (1985) 646.
- [39] R. Schiavilla *et al.*, Nuclear Physics **A449** (1986) 219.
- [40] J.M. Laget, Phys. Lett. **276B** (1992) 398.

- [41] P.E. Ulmer, MCEEP - Monte Carlo for Electro-Nuclear Coincidence Experiments - CEBAF Technical Note - 91 - 101.
- [42] H. Meier-Hadjuk *et al.*, Nuclear Physics **A395** (1983) 332.
- [43] N.E. Cheung *et al.*, submitted to Nucl. Inst. and Meth. in Phys. Res. (1994).
- [44] E. Aprile-Giboni *et al.*, Nucl. Inst. and Meth. **215** (1983) 147.
- [45] M. McNaughton *et al.*, Nucl. Inst. and Meth. **241** (1985) 435.

List of Participants

A. Afanasev, F.T. Baker, L. Bimbot, W. Bertozzi, E.J. Brash, H. Breuer, J. Calarco, C.C. Chang, N.S. Chant, J.P. Chen, D. Dale, B.C. Doyle, J.E. Ducret, M. Epstein, V. Ganenko, A. Gasparian, S. Gilad, R. Gilman, A. Glamazdin, C. Glashausser, V. Gorbenko, C. Howell, G. Huber, M. Jones, G. Kumbartzki, G. Lolos, R. Lourie, P. Markowitz, R. Michaels, S. Nanda, Z. Papandreou, V. Punjabi, C.F. Perdrisat, R. Ransome, P.G. Roos, P.M. Rutt, A. Saha, A. Sarty, P. Sorokin, P.E. Ulmer, H. Voskanyan, L. Weinstein, B. Wojtsekhowski, J.C. Yang.

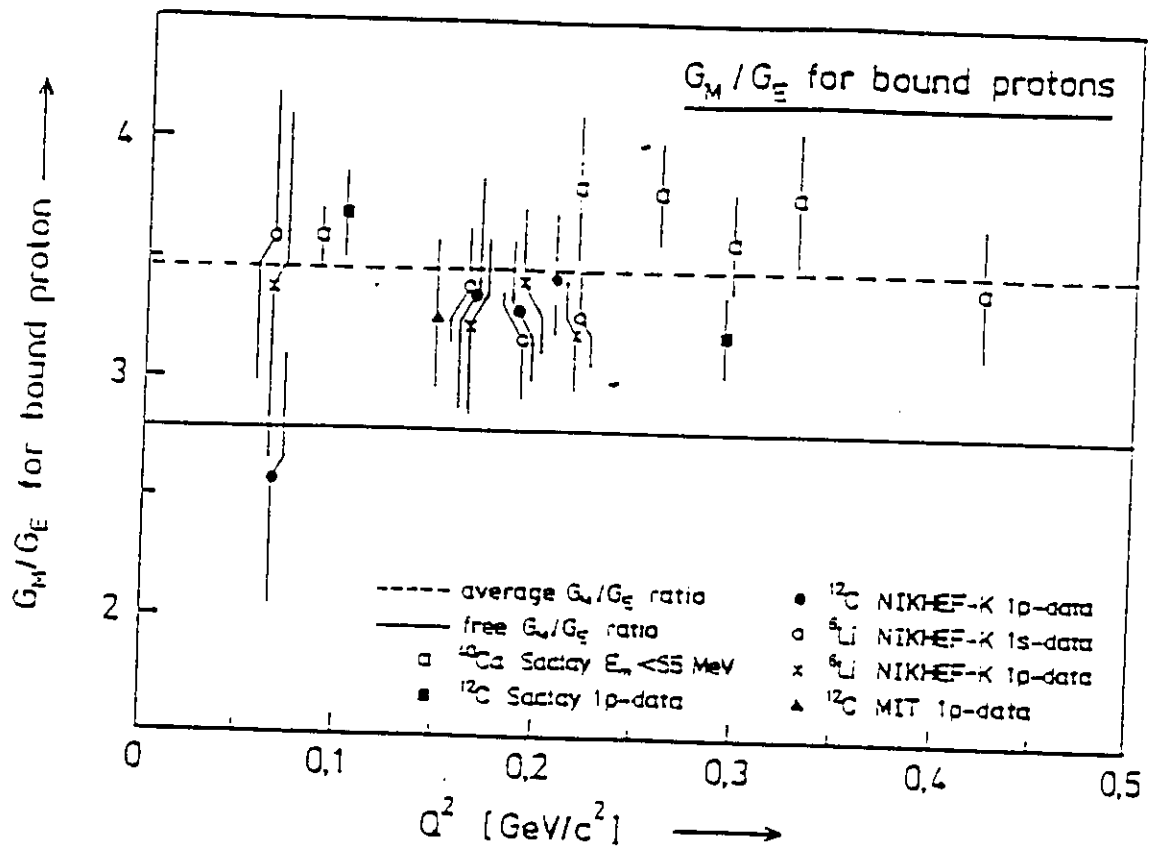


Figure 1. The Ratio of Electromagnetic Form Factors of Bound Protons in Nuclei (G_M^p / G_E^p).

$$E_e = 4.0 \text{ GeV}, Q^2 = 0.8 \text{ (GeV/c)}^2$$

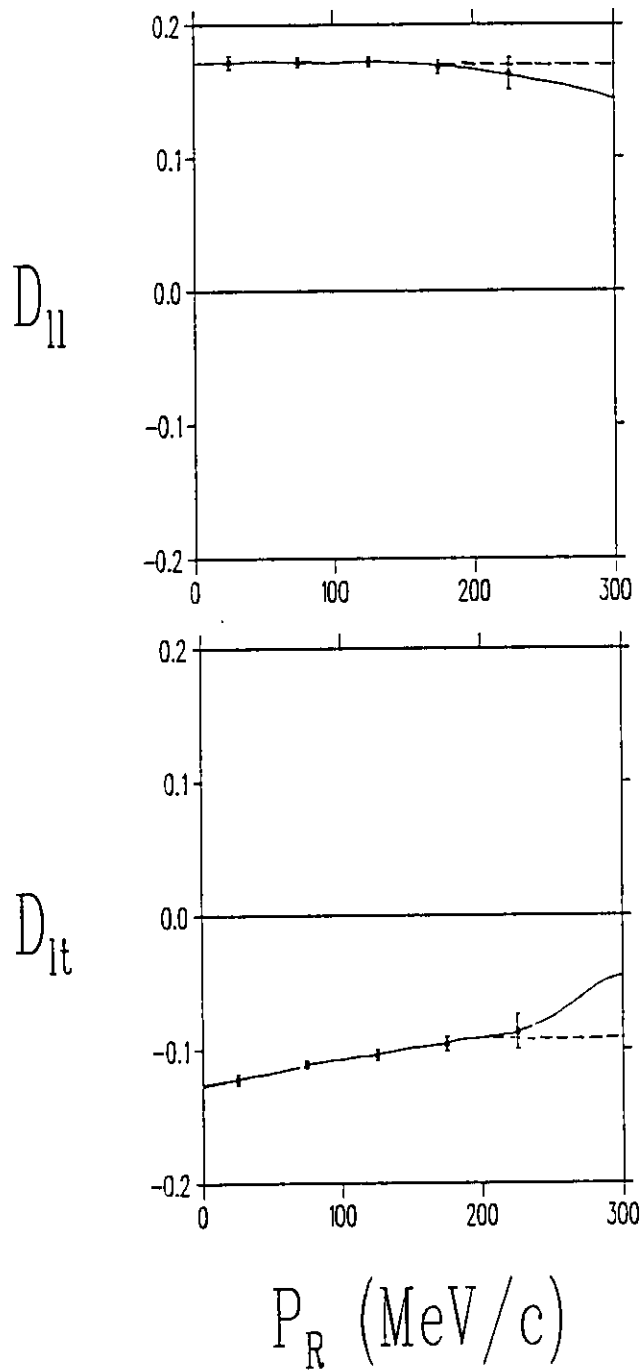


Figure 2. Spin Transfer Coefficients, D_{11} (2a) and D_{1t} (2b), for the ${}^3\text{He}(\bar{e}, e'\bar{p})d$ Reaction.

The solid curve is the calculation of Laget [24] including FSI and MEC effects. The dashed curves have these effects removed. The error bars shown are the planned statistical uncertainties for the experiment.

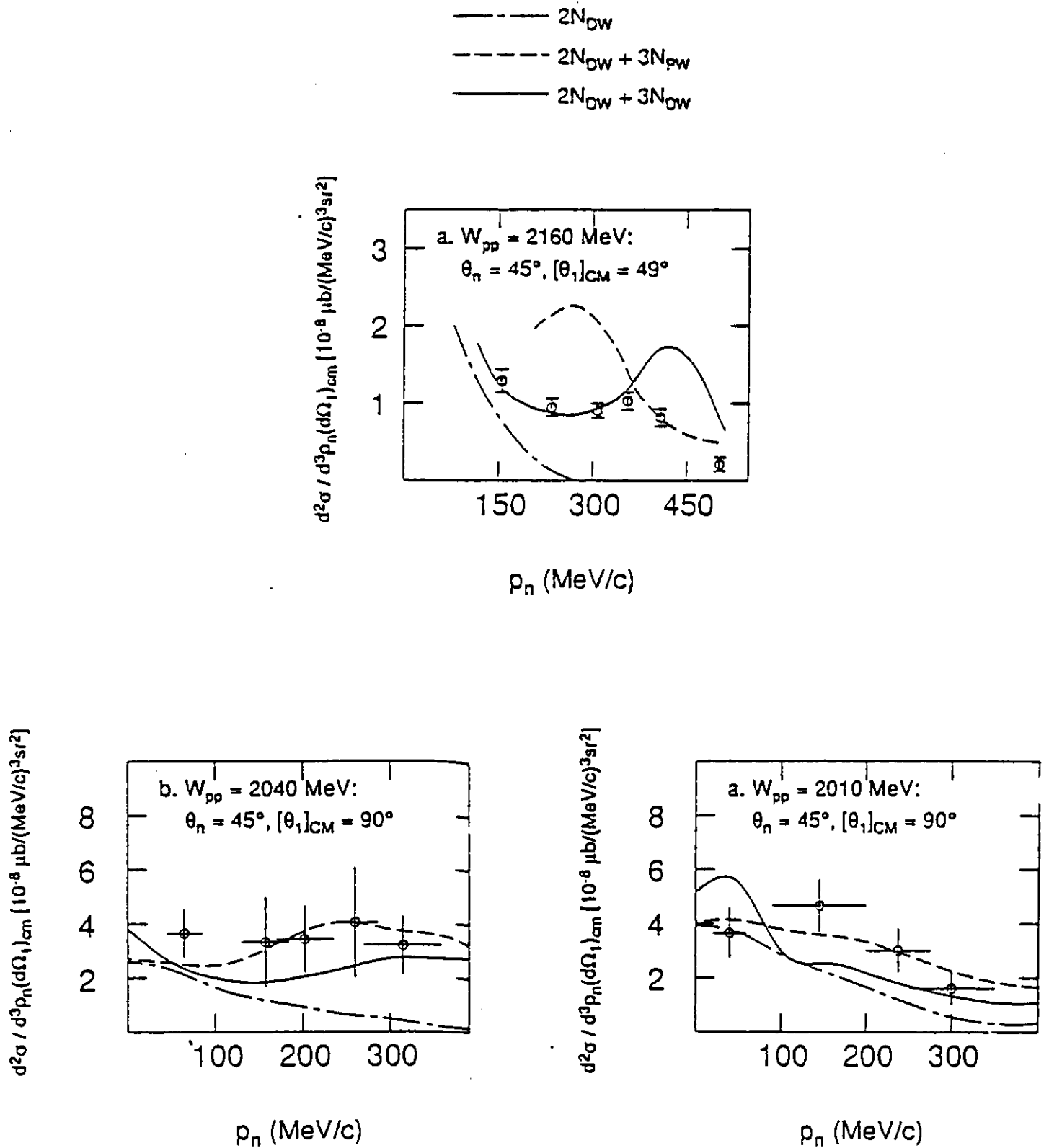


Figure 3. Recent Cross-Section Measurements in the ${}^3\text{He}(\gamma,pp)$ Reaction.

The data in the upper figure are from Audit *et al.* [31]. The data in the lower figures are from Sarty [30]. The explanations of the curves may be found in the text.

S'- State Probability

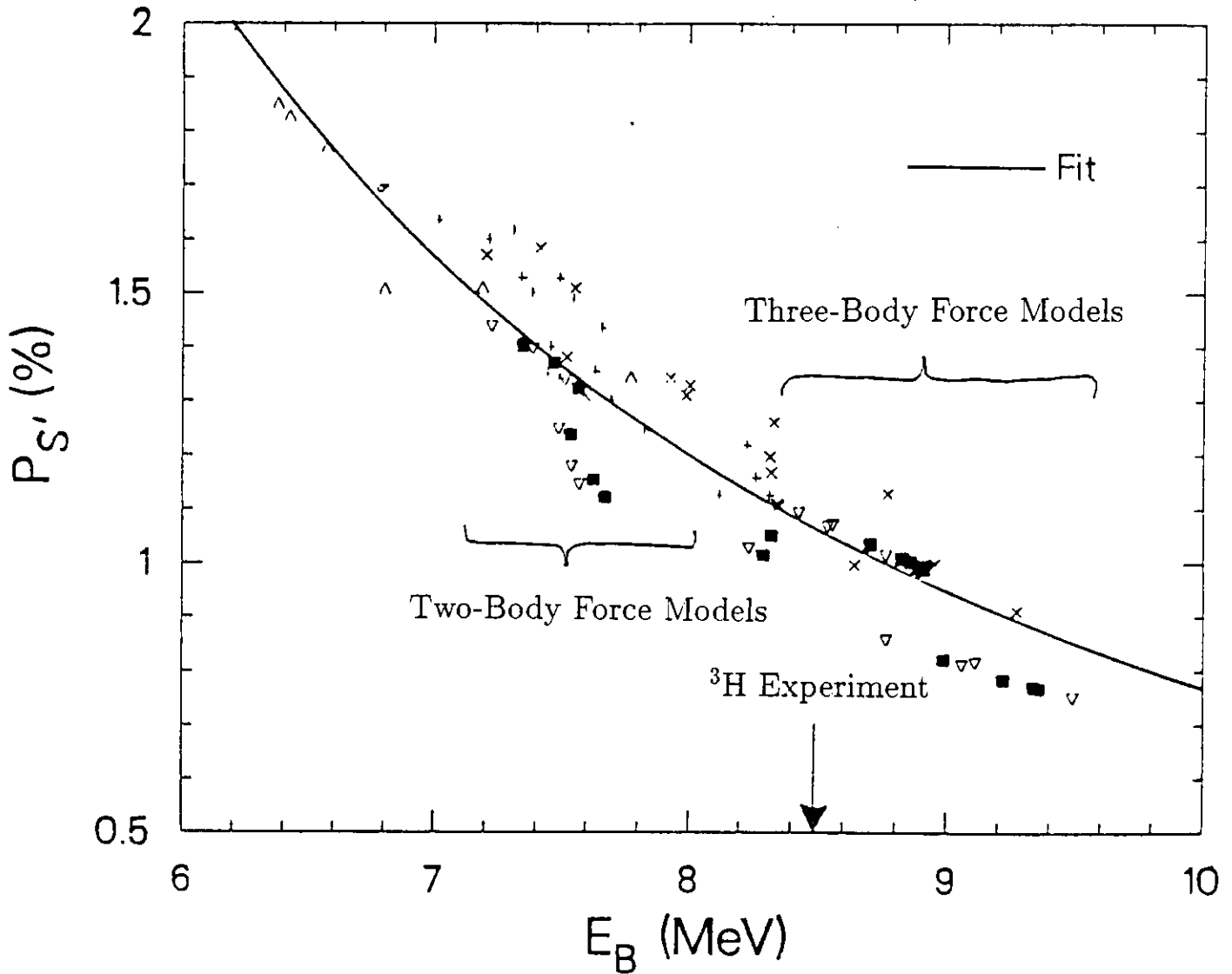


Figure 4. The S'-State Probability in ${}^3\text{H}$

The results shown are for various theoretical models. The fit follows the form $P_{S'} \sim (E_B)^{-2.1}$.

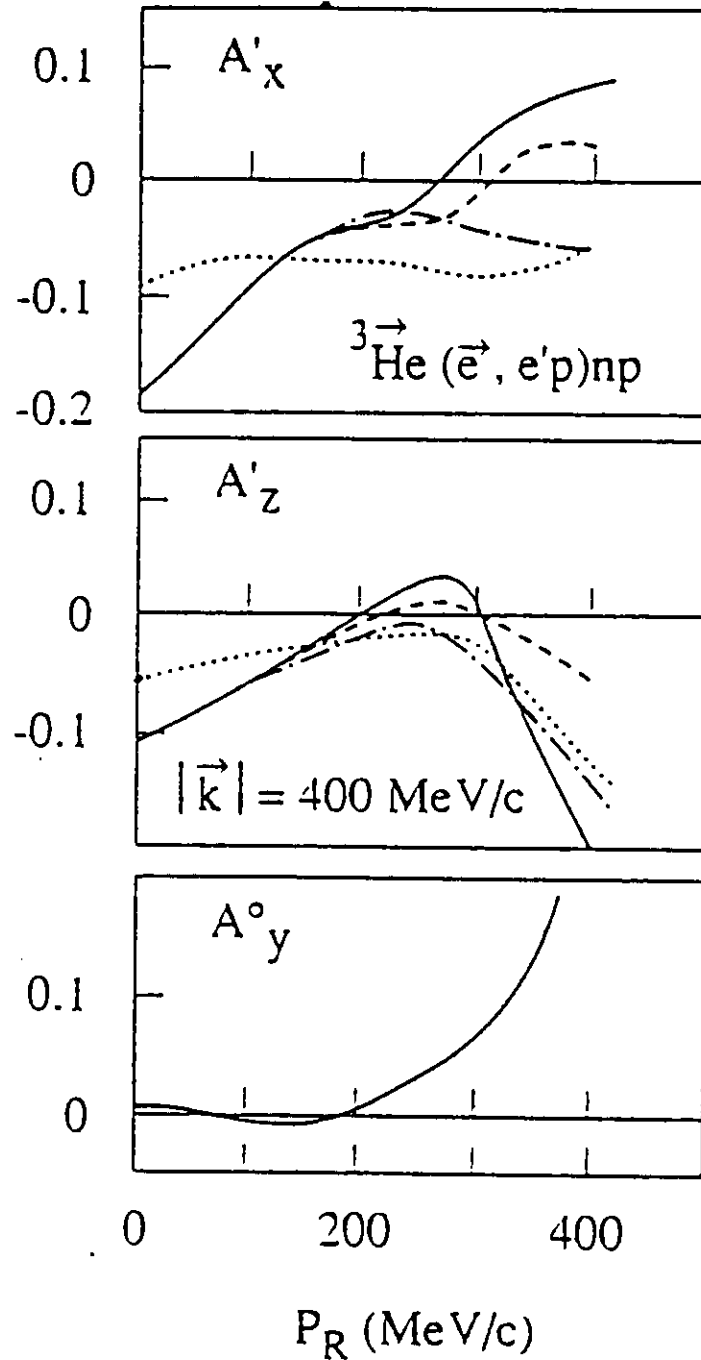


Figure 5. Target Related Asymmetries in the ${}^3\text{He}(\vec{e}, e'p)pn$ Reaction.

While the solid, long-dashed, and dash-dot curves include the S' -state contribution to the ${}^3\text{He}$ wavefunction, the dotted curves are for $P_{S'}=0$.

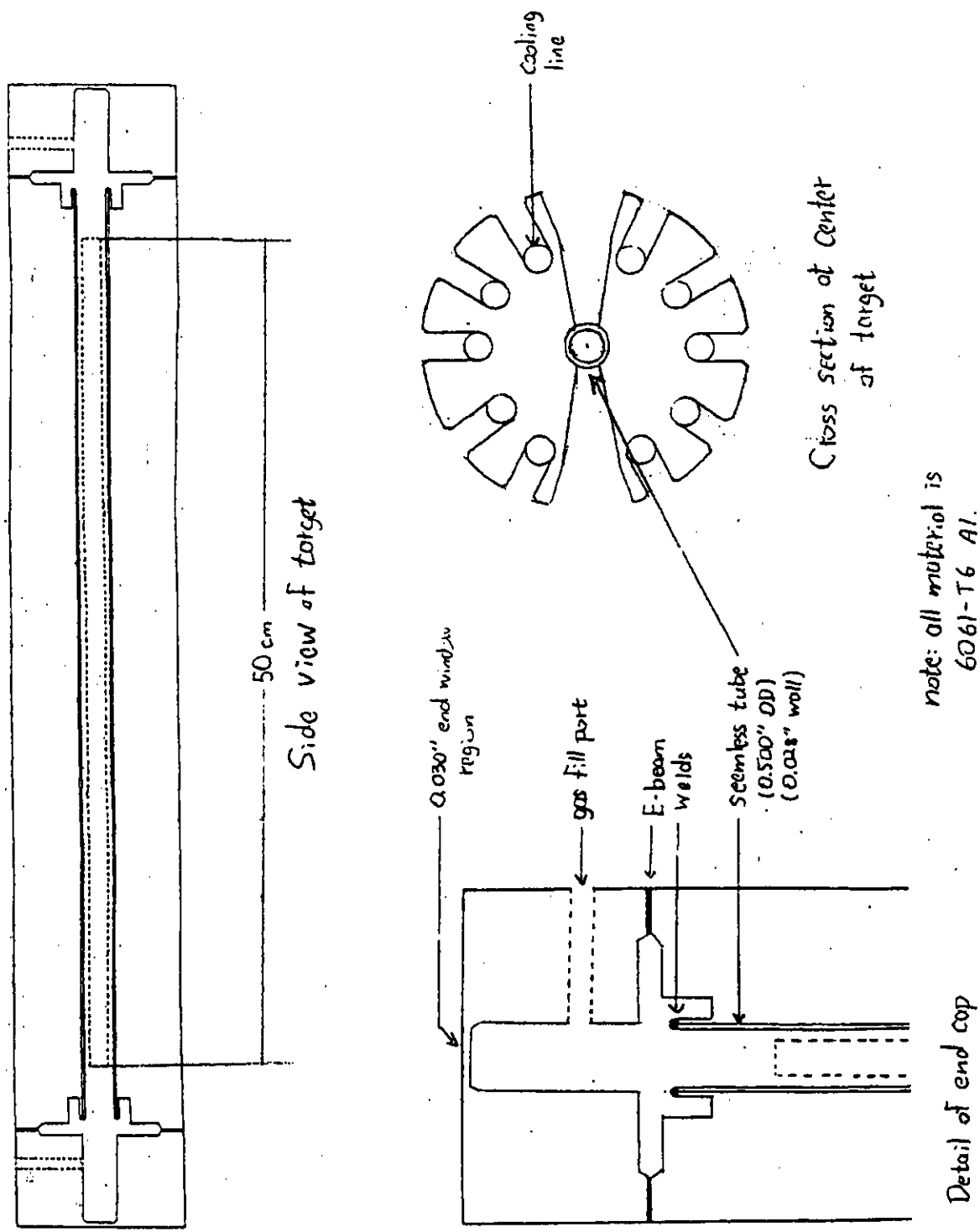


Figure 6. Conceptual Cartoon of the Rutgers High Pressure Gas Target Cell.

HAZARD IDENTIFICATION CHECKLIST

CEBAF Proposal No.: _____

Date: _____

(For CEBAF User Liaison Office use only.)

Check all items for which there is an anticipated need.

<p>Cryogenics</p> <p>_____ beamline magnets</p> <p>_____ analysis magnets</p> <p>_____ target</p> <p>type: _____</p> <p>flow rate: _____</p> <p>capacity: _____</p>	<p>Electrical Equipment</p> <p>_____ cryo/electrical devices</p> <p>_____ capacitor banks</p> <p>_____ high voltage</p> <p>_____ exposed equipment</p>	<p>Radioactive/Hazardous Materials</p> <p>List any radioactive or hazardous/toxic materials planned for use:</p> <p>_____</p> <p>_____</p> <p>_____</p>
<p>Pressure Vessels</p> <p><u>1.128 cm</u> inside diameter</p> <p><u>150 atm</u> operating pressure</p> <p><u>Al</u> window material</p> <p><u>.076 cm</u> window thickness</p> <p>These are for ³He sealed cell.</p> <p>Second cell with 10 atm H₂ with identical physical dimensions.</p>	<p>Flammable Gas or Liquids</p> <p>type: <u>H₂</u></p> <p>flow rate: <u>φ</u></p> <p>capacity: <u>60 cm³</u> (sealed H₂ cell)</p> <p>Drift Chambers</p> <p>type: _____</p> <p>flow rate: _____</p> <p>capacity: _____</p>	<p>Other Target Materials</p> <p>_____ Beryllium (Be)</p> <p>_____ Lithium (Li)</p> <p>_____ Mercury (Hg)</p> <p>_____ Lead (Pb)</p> <p>_____ Tungsten (W)</p> <p>_____ Uranium (U)</p> <p>_____ Other (list below)</p> <p>_____</p> <p>_____</p>
<p>Vacuum Vessels</p> <p>_____ inside diameter</p> <p>_____ operating pressure</p> <p>_____ window material</p> <p>_____ window thickness</p>	<p>Radioactive Sources</p> <p>_____ permanent installation</p> <p>_____ temporary use</p> <p>type: _____</p> <p>strength: _____</p>	<p>Large Mech. Structure/System</p> <p>_____ lifting devices</p> <p>_____ motion controllers</p> <p>_____ scaffolding or</p> <p>_____ elevated platforms</p>
<p>Lasers</p> <p>type: _____</p> <p>wattage: _____</p> <p>class: _____</p> <p>Installation:</p> <p>_____ permanent</p> <p>_____ temporary</p> <p>Use:</p> <p>_____ calibration</p> <p>_____ alignment</p>	<p>Hazardous Materials</p> <p>_____ cyanide plating materials</p> <p>_____ scintillation oil (from)</p> <p>_____ PCBs</p> <p>_____ methane</p> <p>_____ TMAE</p> <p>_____ TEA</p> <p>_____ photographic developers</p> <p>_____ other (list below)</p> <p>_____</p> <p>_____</p>	<p>General:</p> <p>Experiment Class:</p> <p>_____ Base Equipment</p> <p><input checked="" type="checkbox"/> Temp. Mod. to Base Equip.</p> <p>_____ Permanent Mod. to Base Equipment</p> <p>_____ Major New Apparatus</p> <p>Other: <u>Targets will be mounted on solid target ladder in Hall A scattering chamber</u></p>

LAB RESOURCES REQUIREMENTS LIST

CEBAF Proposal No.: _____

(For CEBAF User Liaison Office use only.)

Date: _____

List below significant resources — both equipment and human — that you are requesting *from CEBAF* in support of mounting and executing the proposed experiment. Do not include items that will be routinely supplied to all running experiments, such as the base equipment for the hall and technical support for routine operation, installation, and maintenance.

Major Installations (either your equip. or new equip. requested from CEBAF)

1. modifications to scattering chamber - water cooling lines into/out of scattering chamber - gas fill/vent lines into/out of scattering chamber

2. modifications to solid target ladder to mount high pressure gas target cells.

New Support Structures: _____

Data Acquisition/Reduction

Computing Resources: _____

New Software: _____

Major Equipment

Magnets _____

Power Supplies _____

Targets _____

Detectors _____

Electronics _____

Computer Hardware _____

Other _____

Other

